Optical Properties of metallic ferromagnet $Fe_{1/3}TaS_2$

Shiyu Fan, Department of physics, University of Tennessee

Abstract

We bring together optical spectroscopy and first principles calculations to reveal the electronic properties of the chiral ferromagnet $Fe_{1/3}TaS_2$. Signatures of chirality are superimposed upon a complex free carrier response that emanates from both Ta and Fe bands. These include a honeycomb charge density pattern in the Fe layer and a hole electron pocket crossover at the K-point, low energy excitations between spin split bands that cross the Fermi surface, and clustered rather than well-separated on-site and charge transfer excitations. These findings advance the understanding of intercalation and symmetry breaking on the fundamental excitations in metallic chalcogenides.

Introduction

Research on engineered superlattice materials has blossomed in recent years due to the discovery of unexpected properties deriving from interface[1]. Naturally occurring superlattices like intercalated oxides and chalcogenides are of contemporary interest as well. The chiral ferromagnet $Fe_{1/3}TaS_2$ attracted our attention in this context. This system is based upon 2H-TaS_2 and has a set of stable, well-ordered intercalation plateaus Fe_xTaS_2 at x=1/4 and 1/3 [Fig. 1(a-c)][2]. The pattern of Fe centers is responsible for the non-centrosymmetric, chiral space group of the x=1/3 system. Intercalation suppresses the charge density wave transitions[3], and magnetic transitions arise at 160 and 35 K for the x=1/4 and 1/3 materials, respectively[4]. Moreover, the atomically thin Fe layers in $FexTaS_2$ display fascinating domain wall symmetries and domain patterns[4]. In this work, we show there is a strong influence of the Fe layer on the properties of the compound, perhaps stronger than what would be expected for van der Waals interlayer bonding. The chiral structure modified the electronic properties profoundly.

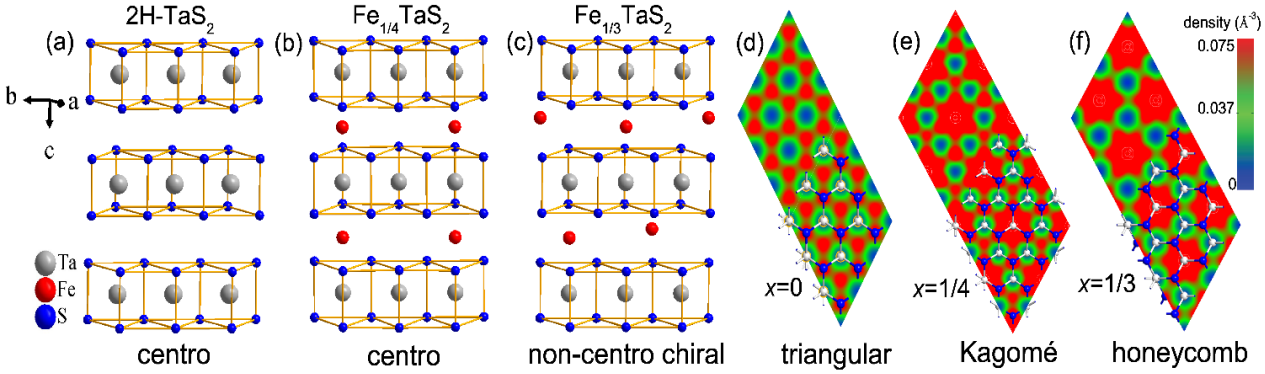

FIG. 1. (a) Crystal structure of 2H-TaS_2 in the centrosymmetric $P6_3/mmc$ space group[5]. (b) $Fe_{1/4}TaS_2$ also belongs to the $P6_3/mmc$ space group[4]. Each Fe center is octahedrally coordinated by six S^{2-} atoms. Stacking along c is AA type, yielding an expanded $2a\times2a$ superlattice. (c) The structure of $Fe_{1/3}TaS_2$ is non-centrosymmetric and chiral (space group $P6_322$)[4]. Stacking along c is alternating (AB) type, yielding a $\sqrt{3}a\times\sqrt{3}a$ superlattice. (d, e, f) Projected charge density in the Fe plane for 2H-TaS2, $Fe_{1/4}TaS_2$, and $Fe_{1/3}TaS_2$[2].

Method

Single crystals of Fe_xTaS_2 (x=1/4 and 1/3) were grown by chemical vapor transport techniques[4]. We measured ab-plane reflectance using a series of spectrometers (4 meV-6.5 eV; 4.2-300 K) and employed a Kramers-Kronig analysis to extract the optical constants. Traditional peak fitting techniques were also employed as appropriate. Computational work was performed using Density Functional Theory provided by Atomistix Toolkit[6]. Using a spin-polarized generalized gradient approach with an on-site potential (SGGA+U), the electronic structure, density of states (DOS), and electron density were determined. The on-site potential localizes the Fe electrons that contribute to the overall magnetic moment; we find 3.8 μ_B.

Result and discussion

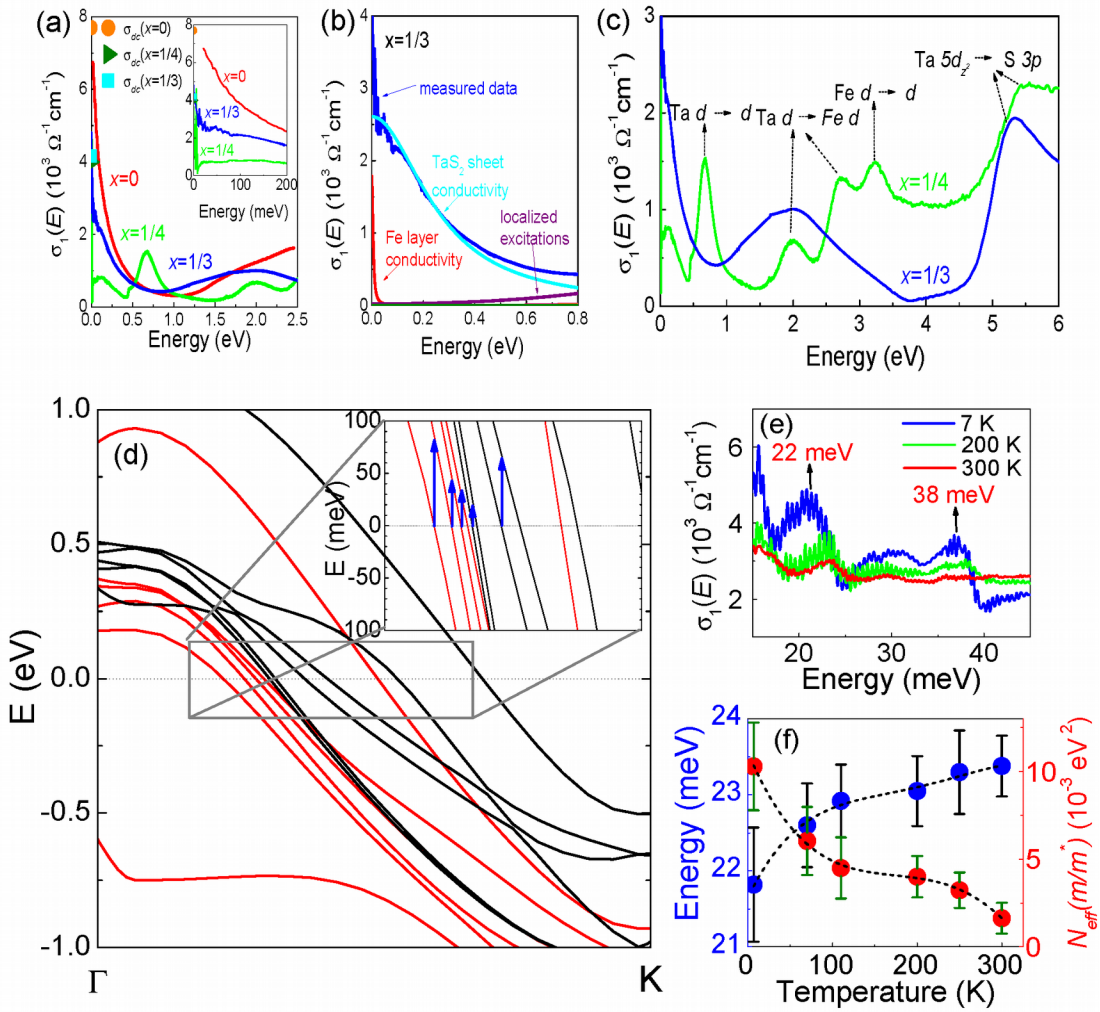

Fig. 2 (a) Optical conductivity of these three materials with x=0, 1/4, and 1/3. Literature values of the dc
Conductivity[7-9] are also plotted; $\sigma_1(E)$ extrapolates to these values reasonably well, 2H-TaS_2 is reproduced from Ref 10. (b) Close-up view of the two Drude oscillators needed to fit the response of $Fe_{1/3}TaS_2$. (c) Optical conductivity of $Fe_{1/4}TaS_2$ and $Fe_{1/3}TaS_2$ highlighting the difference in the localized excitations. (d) Calculated spin-split bands at x=1/3. (e) Low

energy excitations at x=1/3. (f) Oscillator strength and peak position vs temperature at x=1/3.

Figure 2 summarizes the optical data[2]. All samples are metallic as evidenced by the Drude response at low energies. Intercalation dramatically suppresses the metallic character. Furthermore, it also generates a second Drude response at very low energy (Fig. 2 (b)), which is related to the Fe layer conductivity because of a small fraction of Fe density of state around the Fermi level (Fig. 3 (b,c)). Electron density patterns (Fig. 1 (d-f)) also confirmed the two Drude response due to the increasing electron density at the Fe plane between the van der Waals gap. In addition, the increasing Fe concentration sweeps the observed 1 eV bands at x=1/4 level (Fig. 3 (b)) upward to 1.8 eV (Fig. 3 (c)), inducing hybridization to the Ta bands. These bands are relatively flat in the x=1/4 compound but more dispersive at the x=1/3 level, leading to the weaker metallicity of x=1/4 system and the clustered excitation at x=1/3 rather well-seperated excitation at x=1/4. Another important finding is the chiral structure in the x=1/3 compound modifying the electronic structure profoundly. By comparing the K-point at the band structures (Fig 3) of these three different systems, a hole → electron pocket crossover takes place due to the symmetry-breaking effect. This effect also has evidence in the electron density patterns (Fig 1 (d-f)). Since the Fe pattern breaks the inversion center, the Fe layer itself gains symmetry, inducing a charge density pattern changes from a Kagome pattern with a 3-fold symmetry to a honeycomb pattern with a 6-fold symmetry, which causes a hole to electron pocket crossover at the K-point. Furthermore, the breaking of the inversion center also generates the spin splitting bands around the Fermi level at x=1/3 material. Figure 2 (d,e) displays the predicted spin-splits bands from DFT and the observed peaks of the optical data. The energy of these low energy excitations is consistent with the theory. Those peaks are not assigned as phonons because the phonons are expected to be screened by the strong metallic background. However, those excitations are neither predicted or observed in the centrosymmetric systems, which indicates the spin-splitting is related to the symmetry-breaking effect.

Fig. 3: Calculated electronic band structure and DOS (total, partial, and local) for (a) 2H-TaS_2, (b) $Fe_{1/4}TaS_2$, and (c) $Fe_{1/3}TaS_2$. The black and red bands in the electronic structure and the solid and dashed lines in the DOS plots denote the spin-up and spin-down channels, respectively[2].

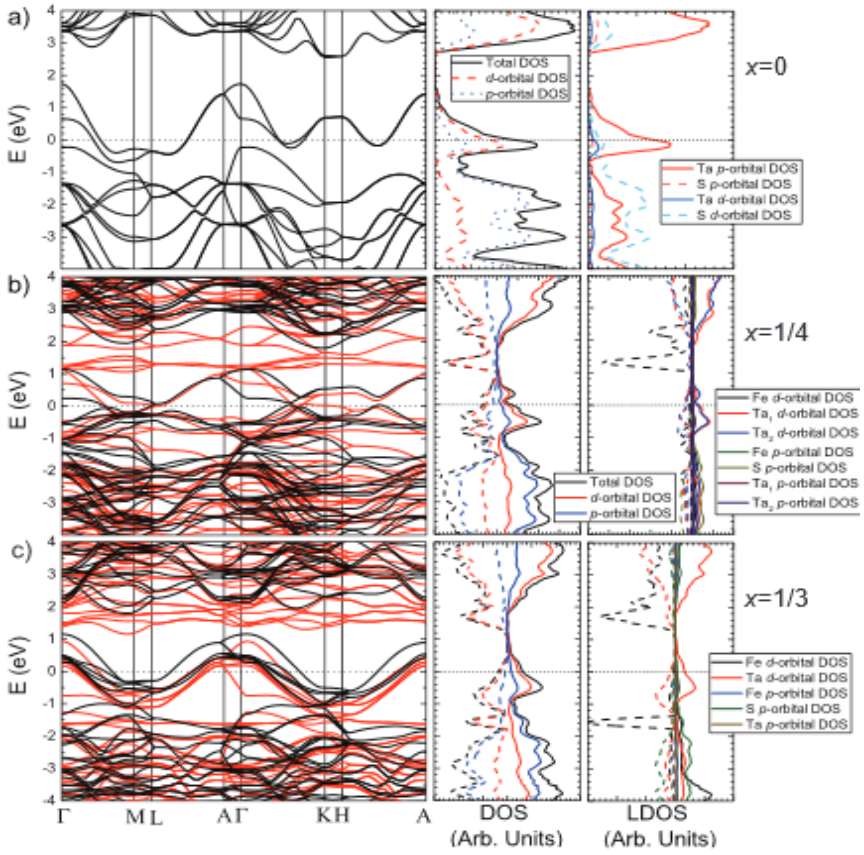

References:

1. H. Y. Hwang, Y. Iwasa, M. Kawasaki, B. Keimer, N. Nagaosa, and Y. Tokura, Nat. Mater. **11**, 103 (2012).
2. S. Fan, I. Manuel, Amal al-Wahish, K. R. O'Neal, K. A. Smith, C. J. Won, J. W. Kim, S. -W. Cheong, J. T. Haraldsen, and J. L. Musfeldt, Phys. Rev. B , **96,** 205119 (2017).
3. S. Mankovsky, K. Chadova, D. Kodderitzsch, J. Minar, H. Ebert, and W. Bensch, Phys. Rev. B **92**, 144413 (2015).
4. Y. Horibe, J. Yang, Y. H. Cho, X. Luo, S. B. Kim, Y. S. Oh, F. T. Huang, T. Asada, M. Tanimura, D. Jeong, and S. W. Cheong, J. Am. Chem. Soc. **136,** 8368 (2014).
5. A. Meetsma, G. A. Wiegers, R. J. Haange, and J. L. de Boer, Acta Cryst. C **46**, 1598 (1990).
6. J. M. Soler, E. Artacho, J. D. Gale, A. Garcia, J. Junquera, P. Ordejon, and D. Sanchez-Portal, J. Phys.: Condens. Matter **14**, 2745 (2002).
7. S. S. P. Parkin and R. H. Friend, Physica **99b**, 219 (1980).
8. J. G. Checkelsky, M. Lee, E. Morosan, R. J. Cava, and N. P. Ong, Phys. Rev. B **77**, 014433 (2008).
9. M. Naito and S. Tanaka, J. Phys. Soc. Jpn. **51**, 219 (1982).
10. W. Z. Hu, G. Li, J. Yan, H. H. Wen, G. Wu, X. H. Chen, and N. L. Wang, Phys. Rev. B **76**, 045103 (2007).

Supplemental information:

The chiral structure of $Fe_{1/3}TaS_2$ system (images are from Ref 4.):

The following figure exhibits the unit cell structures of $Fe_{1/4}TaS_2$ and $Fe_{1/3}TaS_2$. The Fe atoms are intercalated between two TaS_2 prism in the van der waals gap. The stacking pattern of Fe atoms are alternating in the x = 1/3 case (AB) type, which breaks the inversion center of the space group and make the whole system non-centrosymmetric. The bottom right figure shows the top view of the crystal structure on x = 1/3 sample. The three sulfur atoms which surrounded the center Fe atom are distorted due to the non-uniformly distributed neighbouring Ta atoms. The bottom left figure exhibits the side view of a unit cell of $Fe_{1/3}TaS_2$ material. The mirror image of the unit cell cannot be overlapped with its original structure because of the distortion of sulfur atoms reverse the direction during the mirror reflection. This brings the chirality to the system.

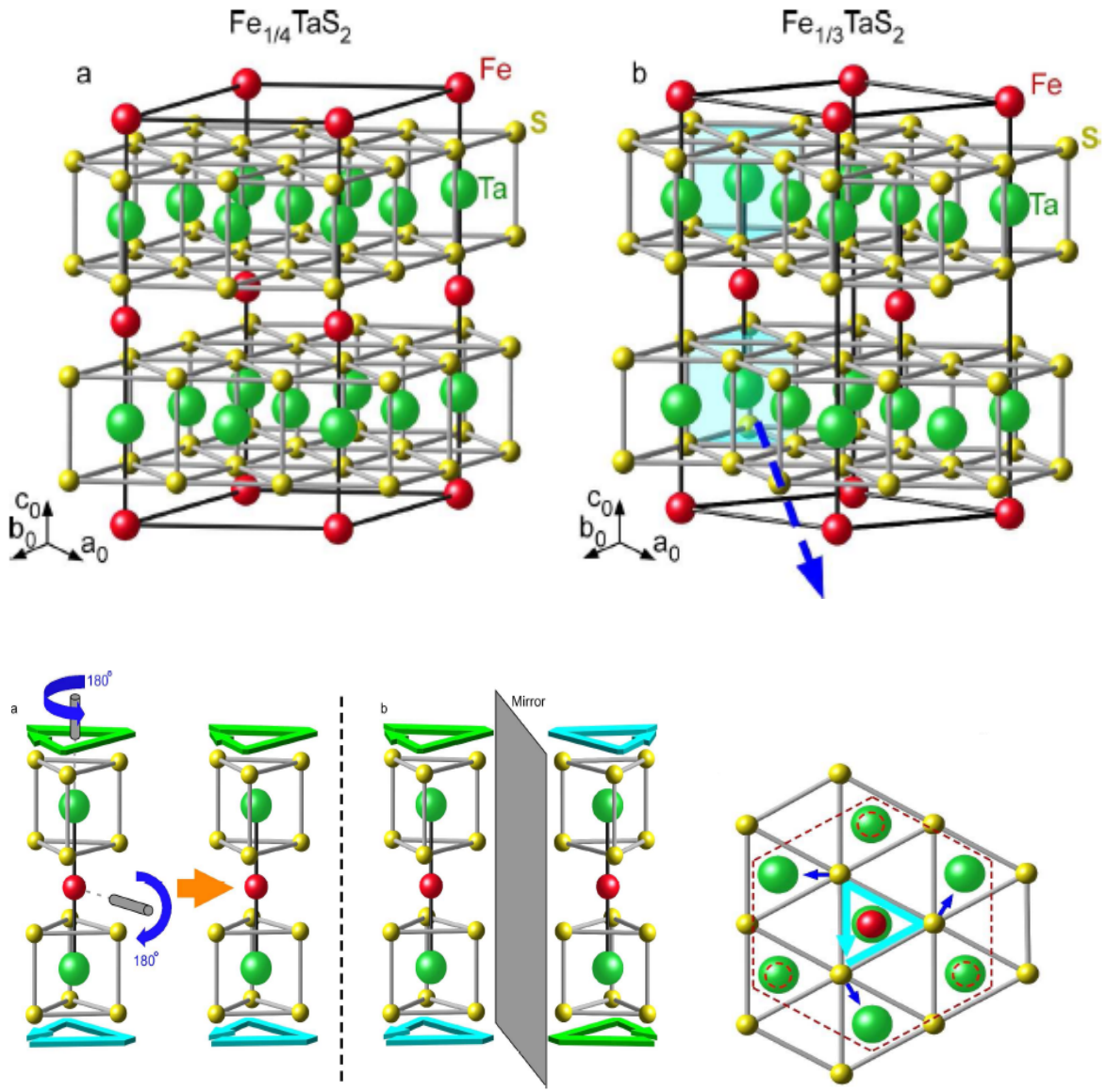
$Fe_{1/4}TaS_2$
a
Fe
S
Ta
c_0
b_0
a_0
$Fe_{1/3}TaS_2$
b
Fe
S
Ta
c_0
b_0
a_0
a
180°
180°
b
Mirror